

Dual-grid parameter choice method with application to image deblurring

Markus Juvonen^{1*}, Bjørn Jensen¹, Ilmari Pohjola¹,
Yiqiu Dong² and Samuli Siltanen¹

¹*University of Helsinki, Finland*

²*Technical University of Denmark, Denmark*

April 2025

Abstract

Variational regularization of ill-posed inverse problems is based on minimizing the sum of a data fidelity term and a regularization term. The balance between them is tuned using a positive regularization parameter, whose automatic choice remains an open question in general. A novel approach for parameter choice is introduced, based on the use of two slightly different computational models for the same inverse problem. Small parameter values should give two very different reconstructions due to amplification of noise. Large parameter values lead to two identical but trivial reconstructions. Optimal parameter is chosen between the extremes by matching image similarity of the two reconstructions with a pre-defined value. Efficacy of the new method is demonstrated with image deblurring using measured data and two different regularizers.

1 Introduction

Variational regularization is a fundamental solution technique for ill-posed inverse problems. The basic idea is to minimize a penalty functional with two terms: a data fidelity term and a regularization term, the former ensuring solutions remain close to the measured data and the latter modeling *a priori* information about the unknown [7]. The balance between the two terms is tuned using a positive regularization parameter, whose automatic choice remains an open question in general. We introduce a novel approach for parameter choice based on the use of two slightly different computational models.

Consider a forward problem model

$$m = \mathcal{A}(f) + \varepsilon, \tag{1}$$

*email: markus.juvonen@helsinki.fi

where m is the observed measurement data, f is the underlying unknown true target, ε is measurement noise and \mathcal{A} is the measurement model. Our formulation of variational regularization is

$$\arg \min_f \|m - \mathcal{A}(f)\|_2^2 + \alpha \mathcal{R}(f) \quad (2)$$

where $\alpha > 0$ is the regularization parameter. The data fidelity term $\|m - \mathcal{A}(f)\|_2^2$ penalizes vectors f for not matching the measured data, and the regularizer \mathcal{R} should be picked or designed so that the value $\mathcal{R}(f) > 0$ is larger for any f that are not expected in light of any *a priori* information. We focus on choosing α automatically in an optimal way.

Many methods have been suggested in the literature: discrepancy principles [1, 25, 21], cross-validation [12, 26], the L-curve method [9], sparsity matching [8, 18, 17, 13], multigrid method [14], residual whiteness principle [16] and others [4, 6, 3, 11, 5]. However, while some of the above methods might work for a given application, it may not be useful for slightly different applications. In practice, automatic parameter choice remains a challenge.

We introduce a new parameter choice principle, similar in spirit to the multiresolution idea in [14], but simpler and more general. Our idea is to use two forward models, both written for the same data m but using different computational grids to represent the unknown f . We then solve the same problem for both grids for multiple parameter values α and compare the structural similarity of the two solutions using SSIM [24]. If the parameter is too small, we expect to have a low similarity between the solutions, as noise is amplified in an ill-posed reconstruction process. However, the similarity should grow with increasing α when the problem is stabilized. We can set a suitable target threshold for the SSIM value and find a good parameter value for the reconstructions as we reach this threshold.

In this paper, we study the new method in the context of image deblurring. Our approach is independent of the regularizer, so we test it with two different ones: Tikhonov regularization [20, 10] and total variation (TV) regularization [19, 22, 15, 23]. We test our method with both simulated and real data and compare the new algorithm with the classical discrepancy principle.

2 Materials and methods

2.1 Dual-grid model for image deblurring

Let us explain our approach in more detail using two-dimensional convolution

$$m = p * f = \int_{\mathbb{R}^2} f(x - y)p(y)dy \quad (3)$$

as the model problem. In (3), measured data is again denoted by m , the unknown is f , and p is a point spread function. Finding f when p is given and m measured is the inverse problem called deconvolution.

Let $s \in \mathbb{R}^2$ be a displacement vector called the *shift*. Define the shifted image f_s and shifted point spread function p_{-s} as follows:

$$f_s(x) = f(x + s), \quad p_{-s}(x) = p(x - s).$$

Substituting $\lambda = y + s$ to (3) we get the shift identity

$$(p * f)(x) = \int_{\mathbb{R}^2} f_s(x - \lambda) p_{-s}(\lambda) d\lambda = (p_{-s} * f_s)(x). \quad (4)$$

Now consider another forward model using the shifted point spread function:

$$m = p_{-s} * g. \quad (5)$$

Assume (unrealistically) that we can solve the inverse problems (3) and (5) perfectly and that the measurement in both cases is the same m . Then (4) implies that the recovered images are related by a shift: $g = f_s$.

Let's move to a more realistic model. Given a blurred pixel image $\mathbf{m} \in \mathbb{R}^{n \times n}$, we use a discrete computational model with periodic boundary conditions:

$$\mathbf{m} = \mathbf{p} \star \mathbf{f} + \mathbf{e} = \mathcal{F}^{-1}(\mathcal{F}(\mathbf{p}) \cdot \mathcal{F}(\mathbf{f})) + \mathbf{e}, \quad (6)$$

where \mathcal{F} is the discrete Fourier transform, $\mathbf{f} \in \mathbb{R}^{n \times n}$ is the sharp image defined on the same pixel grid where \mathbf{m} is given (camera sensor pixels), $\mathbf{p} \in \mathbb{R}^{n \times n}$ is the discrete PSF, and $\mathbf{e} \in \mathbb{R}^{n \times n}$ models random measurement noise. Also, “ \cdot ” in (6) means the pixel-wise Hadamard product.

Denote the length of the side of a square pixel in our grid by $h > 0$. For the rest of this study, we fix the shift vector to be

$$s = [h/2, h/2]^T \in \mathbb{R}^2.$$

Define “half-pixel shift kernels” related to the shift vector s :

$$\mathbf{d}_s = \begin{bmatrix} 0 & 0 & 0 & 0 & 0 \\ 0 & 0 & 0 & 0 & 0 \\ 0 & 1/4 & \mathbf{1/4} & 0 & 0 \\ 0 & 1/4 & \mathbf{1/4} & 0 & 0 \\ 0 & 0 & 0 & 0 & 0 \end{bmatrix}, \quad \mathbf{d}_{-s} = \begin{bmatrix} 0 & 0 & 0 & 0 & 0 \\ 0 & 0 & 1/4 & 1/4 & 0 \\ 0 & 0 & \mathbf{1/4} & 1/4 & 0 \\ 0 & 0 & 0 & 0 & 0 \\ 0 & 0 & 0 & 0 & 0 \end{bmatrix},$$

where there need to be an appropriate amount of zero elements according to image size. The central elements of the kernels are indicated as bold.

Consider two computational models: the camera grid model

$$\mathbf{m} = \mathbf{p} \star \mathbf{f} + \mathbf{e}, \quad (7)$$

and the shifted model

$$\mathbf{m} = \mathbf{p}_{-s} \star \mathbf{g} + \mathbf{e}, \quad (8)$$

where $\mathbf{g} \in \mathbb{R}^{n \times n}$ is the desired sharp image *on a shifted pixel grid* and $\mathbf{p}_{-s} = \mathbf{p} \star \mathbf{d}_{-s}$ is the shifted PSF. Note that the data \mathbf{m} is the same in both models (7) and (8).

Solve the inverse problems (7) and (8) by regularization with parameter $\alpha > 0$ and regularizer $\mathcal{R} : \mathbb{R}^{n \times n} \rightarrow \mathbb{R}^+$, yielding reconstructions

$$\mathbf{f}^{(\alpha)} = \arg \min_{\mathbf{f} \in \mathbb{R}^{n \times n}} \|\mathbf{m} - \mathbf{p} \star \mathbf{f}\|_F^2 + \alpha \mathcal{R}(\mathbf{f}), \quad (9)$$

$$\mathbf{g}^{(\alpha)} = \arg \min_{\mathbf{g} \in \mathbb{R}^{n \times n}} \|\mathbf{m} - \mathbf{p}_{-s} \star \mathbf{g}\|_F^2 + \alpha \mathcal{R}(\mathbf{g}), \quad (10)$$

where $\|\cdot\|_F$ denotes the Frobenius norm. The above discussion of the continuous problem suggests that with any large enough $\alpha > 0$ we should have $\mathbf{g}^{(\alpha)} \approx \mathbf{f}^{(\alpha)} \star \mathbf{d}_s$. Consequently the structural similarity of the two images should be high: $\text{SSIM}(\mathbf{g}^{(\alpha)}, \mathbf{f}^{(\alpha)} \star \mathbf{d}_s) \approx 1$.

Furthermore, convolving a properly regularized image $\mathbf{f}^{(\alpha)}$ by \mathbf{d}_s does not change the image much under SSIM. Therefore we get

$$\text{SSIM}(\mathbf{g}^{(\alpha)}, \mathbf{f}^{(\alpha)}) \approx 1.$$

However, with too small parameter $\alpha > 0$ the noise in the measurements is uncontrollably amplified in the reconstruction process, resulting in erratic pixel values in $\mathbf{g}^{(\alpha)}$ and $\mathbf{f}^{(\alpha)}$. The noise components in the two reconstructions are expected to be different because of the randomness behaviour.

We arrive at our research hypothesis:

- If the regularization parameter $\alpha > 0$ is too small, then $\text{SSIM}(\mathbf{g}^{(\alpha)}, \mathbf{f}^{(\alpha)})$ is much smaller than 1, indicating that $\mathbf{f}^{(\alpha)}$ and $\mathbf{g}^{(\alpha)}$ are two very different images due to amplification of noise in the unstable inversion process.
- If $\alpha > 0$ is large enough, then $\text{SSIM}(\mathbf{g}^{(\alpha)}, \mathbf{f}^{(\alpha)})$ is close to 1. Then $\mathbf{g}^{(\alpha)}$ and $\mathbf{f}^{(\alpha)}$ are approximately equal, and so regularization is not too weak.

Our proposed strategy is to pick the smallest α for which $\text{SSIM}(\mathbf{g}^{(\alpha)}, \mathbf{f}^{(\alpha)}) \geq T$, where $T \in (0, 1)$ and close to 1 is a user-defined lower bound for image quality.

To back up the hypothesis, we performed a numerical experiment reported below in Section 3.1.

2.2 Tikhonov regularization

The Tikhonov regularized solution of 9 and 10 is defined on the two grids by:

$$\mathbf{f}^{(\alpha)} = \arg \min_{\mathbf{f} \in \mathbb{R}^{n \times n}} \|\mathbf{m} - \mathbf{p} \star \mathbf{f}\|_F^2 + \alpha \|\mathbf{f}\|_F^2, \quad (11)$$

$$\mathbf{g}^{(\alpha)} = \arg \min_{\mathbf{g} \in \mathbb{R}^{n \times n}} \|\mathbf{m} - \mathbf{p}_{-s} \star \mathbf{g}\|_F^2 + \alpha \|\mathbf{g}\|_F^2 \quad (12)$$

where $\alpha > 0$ is the regularization parameter.

We compute reconstructions using a FFT-based algorithm [10].

2.3 TV regularization

We use the *isotropic* definition of total variation so the TV-regularized solution of 9 and 10 is defined on the two grids by:

$$\mathbf{f}^{(\alpha)} = \arg \min_{\mathbf{f} \in \mathbb{R}^{n \times n}} \|\mathbf{m} - \mathbf{p} \star \mathbf{f}\|_F^2 + \alpha \sum_{i,j=1}^n \sqrt{(D_x \mathbf{f})_{i,j}^2 + (D_y \mathbf{f})_{i,j}^2}, \quad (13)$$

$$\mathbf{g}^{(\alpha)} = \arg \min_{\mathbf{g} \in \mathbb{R}^{n \times n}} \|\mathbf{m} - \mathbf{p}_{-s} \star \mathbf{g}\|_F^2 + \alpha \sum_{i,j=1}^n \sqrt{(D_x \mathbf{g})_{i,j}^2 + (D_y \mathbf{g})_{i,j}^2} \quad (14)$$

where $\alpha > 0$ is the regularization parameter and D_x , D_y denote the horizontal and vertical partial derivative operators, respectively.

We compute TV reconstructions using a standard primal-dual deconvolution solver [2].

2.4 Simulated Data (image with various geometric shapes)

Our test image is a 512x512 sized computer created image with various geometric shapes with edges in several directions and various gray scale values for the shapes. See Figure 1.

The simulated image blur was created using a convolution kernel that has a constant value inside a disc domain and zero outside. We added Gaussian noise that is scaled relative to the norm of the image. Two different noise levels were chosen, one with 4% and another with 8% of noise relative to the image.

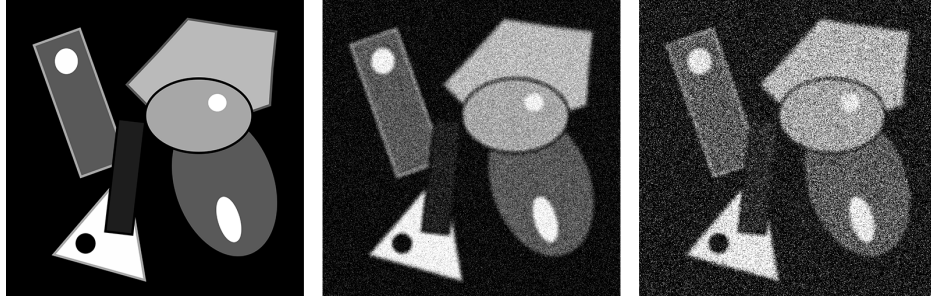


Figure 1: Left: Simulated ground truth with no noise or blur. Middle: Blurred with radius 4 kernel and 4% added noise. Right: Blurred with radius 4 kernel and added 8% noise.

2.5 Real Photographic Data

To test our method on real data we captured two small datasets with a Canon EOS 5D Mark IV camera. For the playing card set a Canon EF 100mm f/2.8 USM Macro lens was attached to the camera and for the books dataset a newer

Canon EF 100mm f/2.8 USM IS Macro lens was used. For both datasets multiple blur (lens misfocus) levels and noise (ISO) levels were captured. The scene was properly exposed each time. To compensate for the change in signal intensity/exposure when increasing the ISO setting the shutter speed was changed accordingly. The camera was mounted on a tripod and the subjects static so the change of shutter speed did not introduce any additional motion blur. For the playing card image the ISO levels were ISO100 for the "ground truth", ISO1600 for the less noisy image and ISO6400 for the more noisy image. For the image with books the ISO levels were ISO100, ISO6400 and ISO25600 accordingly. In both sets a blurred noiseless (ISO100) image was used to estimate the amount of blur i.e. to estimate the radius of the blur kernel. In section 3.2 we will show tests of our method on the following real data examples.

2.6 Real Dataset 1: Playing card

A 1024x1024 pixel sized crop from an image of a regular playing card. We have a ground truth estimate on the left in figure 2. This is a real photograph correctly focused and taken with the lowest possible ISO setting. In the middle we have a slightly blurred and noisier version (ISO1600) of the same scene and on the right the same amount of blur but higher noise level (ISO6400).



Figure 2: Left: "Ground truth", almost noiseless (ISO100). Middle: Slightly blurred, some noise (ISO1600). Right: Slightly blurred, more noise (ISO6400).

2.7 Real Dataset 2: Books

A 1024x1024 pixel sized crop from an image of a stack of books. We have a ground truth estimate on the left in figure 3. This is a real photograph correctly focused and taken with the lowest possible ISO setting. In the middle we have a slightly blurred and noisier version (ISO6400) of the same scene and on the right the same amount of blur but higher noise level (ISO25600).

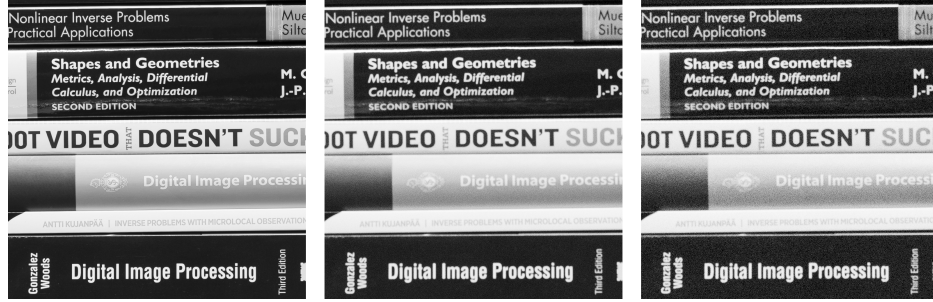


Figure 3: "Ground truth" (ISO100) on the left. Slightly blurred and small noise (ISO6400) in the middle. Slightly blurred and more noise (ISO25600) on the right.

3 Results

3.1 Numerical test of similarity hypothesis

We first computed the SSIM between a set of 230 natural images \mathbf{f} and their shifted versions $\mathbf{f} \star \mathbf{d}_s$. The blue graph in Figure 4 shows that \mathbf{f} is quite different from $\mathbf{f} \star \mathbf{d}_s$ under the SSIM measure. Then we repeated the calculation for denoised versions of those 230 images. (Note that we did not add any noise to the original images before denoising.) The red and orange graphs in Figure 4 show that shifting an image smoothed by Tikhonov or TV regularization does not change the image as much in terms of SSIM.

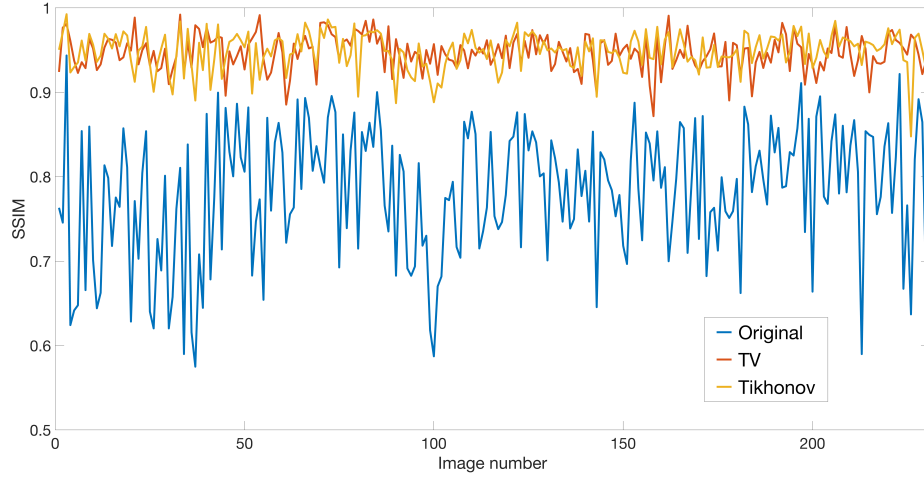


Figure 4: SSIM between images on the two grids. The blue graph indicates that for a regular photograph, a sub-pixel shift causes a significant change in the image as measured by SSIM. However, for images smoothed by Tikhonov or total variation denoising, the change caused by the shift is much weaker: their SSIM values are closer to 1.

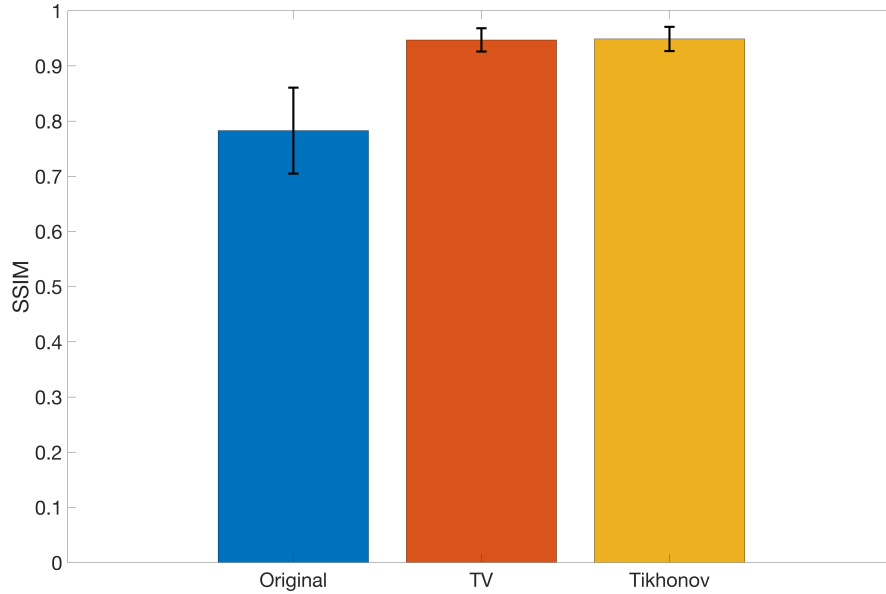


Figure 5: Mean SSIM value between images on the two grids and standard deviation computed for all 230 images in Figure 4.

3.2 Dual-grid parameter selection tests

In this section we present some results of the dual-grid parameter selection method for one simulated and two real photographic data sets. The simulated image data used for this test is presented in section 2.4. The real data sets are presented in sections 2.6 and 2.7.

3.2.1 Simulated image example

First we test the dual-grid approach on a the simulated image example shown in Figure 1. For the simulated images we know that the blur kernel radius is 4 but the added noise makes solving this problem ill-posed. For both regularizers we get the expected behaviour of the SSIM function as seen in Figure 6. We also see that for the lower noise case the selected parameter is in both cases smaller than with higher noise level.

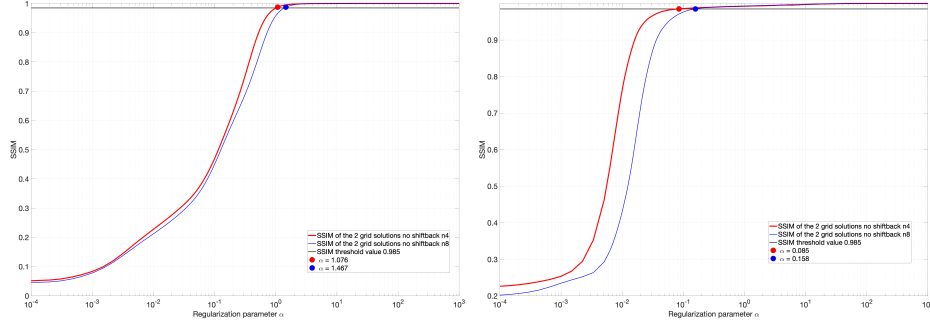


Figure 6: Dual-grid method for parameter choice for the case of simulated images shown in 1. Plotted is the SSIM function between the two solutions $\text{SSIM}(\mathbf{g}^{(\alpha)}, \mathbf{f}^{(\alpha)})$ for two regularizers and two noise amplitudes. Left: Tikhonov regularization. The first regularization parameter after the selected threshold value is $\alpha = 1.076$ for the case with less noise (red curve) and $\alpha = 1.467$ for the higher noise case (blue curve). Right: total variation regularization. The first regularization parameter after the selected threshold value is $\alpha = 0.085$ for the case with less noise (red curve) and $\alpha = 0.158$ for the higher noise case (blue curve).

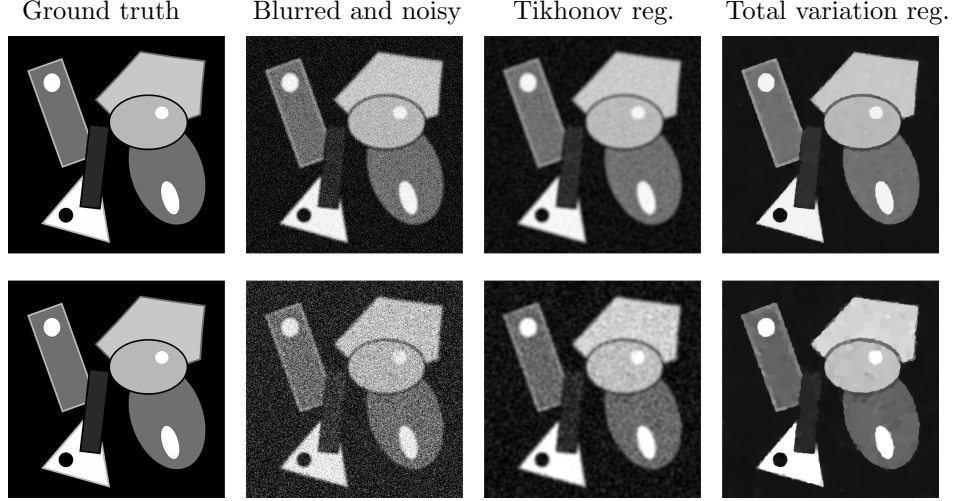


Figure 7: Geometric shapes images and reconstructions with regularization parameter values selected with dual-grid method as seen in Figure 6 . First row: Ground truth, blur radius 4 + noise 4%, Tikhonov regularized, TV. Second row: Ground truth, blur radius 4 + noise 8%, Tikhonov regularized , TV regularized (Tikh threshold .985, TV threshold .985).

3.2.2 Playing card example

For the first real data test we took the playing card image shown in 2. For the real data cases we don't know the exact blur kernel that has caused the blur so we need to estimate it. In this case we ended up with a estimated kernel radius of 6 by measuring how much distinct points have spread after the misfocusing compared to the sharp noisless "ground truth" image. For the tikhonov regularizer we see pretty nicely behaving SSIM functions in Figure 8. For the TV regularized ones we see that the exact point where the SSIM function starts to flatten out is not so well defined. For both regularizers we notice that we actually get a smaller parameter value choice for the higher noise case.

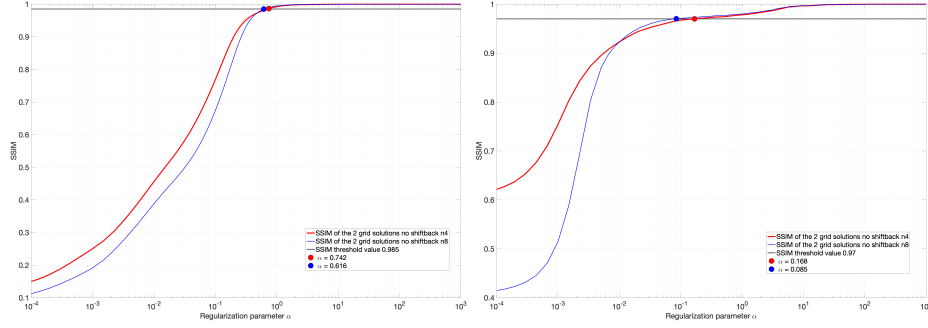


Figure 8: Dual-grid method for parameter choice for the case of the playing card images shown in 2. Plotted is the SSIM function between the two solutions $\text{SSIM}(\mathbf{g}^{(\alpha)}, \mathbf{f}^{(\alpha)})$ for two regularizers and two noise amplitudes. Left: Tikhonov regularization. The first regularization parameter after the selected threshold value is $\alpha = 0.742$ for the case with less noise (red curve) and $\alpha = 0.616$ for the higher noise case (blue curve). Right: total variation regularization. The first regularization parameter after the selected threshold value is $\alpha = 0.168$ for the case with less noise (red curve) and $\alpha = 0.085$ for the higher noise case (blue curve).

3.2.3 Example reconstructions

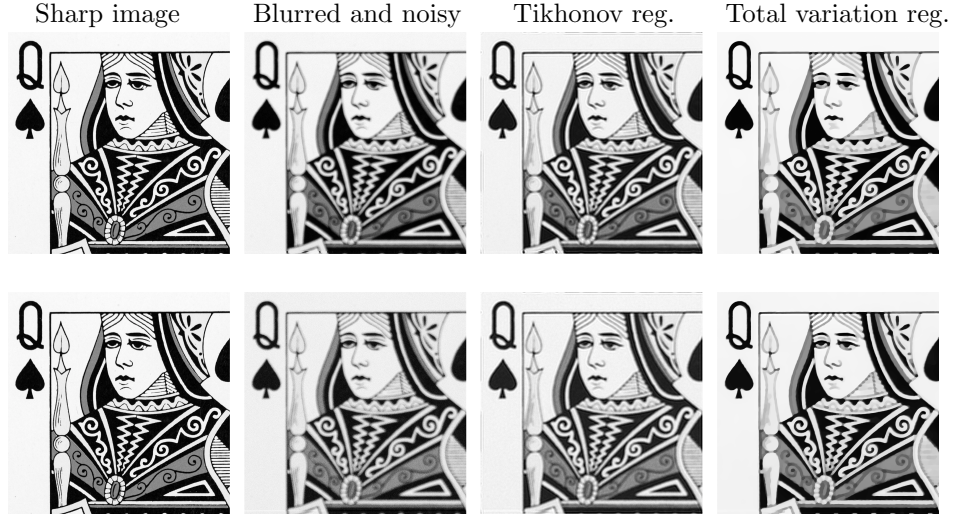


Figure 9: Queen playing card and reconstructions with regularization parameter values selected with dual-grid method as seen in Figure 8. First row: "Ground truth" sharp image (ISO100), blur+little noise(ISO1600), Tikhonov, TV. Second row: "Ground truth" sharp image (ISO100), blur+more noise(ISO6400), Tikhonov, TV. (Tikh threshold .985, TV threshold .97)

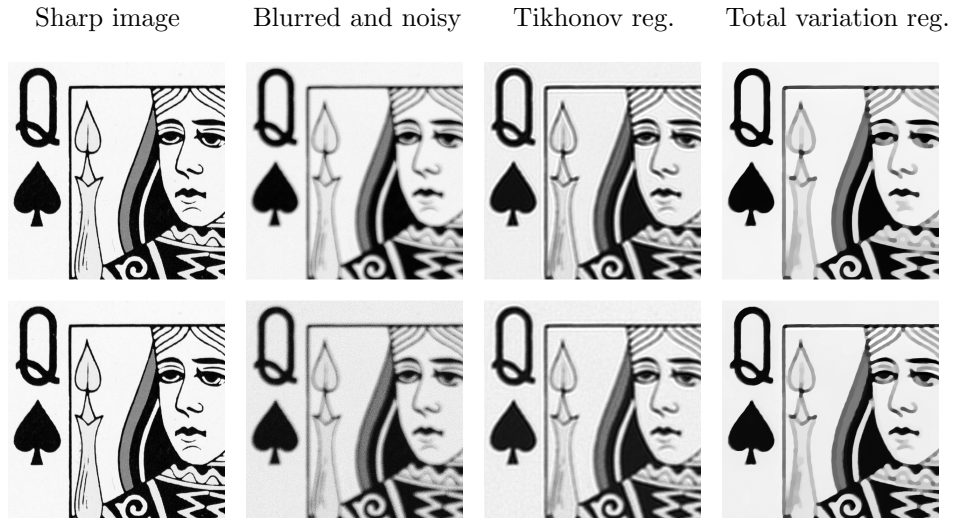


Figure 10: Queen playing card images from Figure 9 cropped for a more detailed view. First row: "Ground truth" sharp image (ISO100), blur+little noise(ISO1600), Tikhonov, TV. Second row: "Ground truth" sharp image (ISO100), blur+more noise(ISO6400), Tikhonov, TV. (Tikh threshold .985, TV threshold .97)

3.2.4 Books image example

As the second real data case we have the books image 3. The blur kernel radius estimation in this case is 5. We see similar behaviour of the SSIM functions to the playing card image case.

In the TV case we clearly notice how the SSIM log plots in Figure 11 don't have the same s-shape but they grow more gradually from a value of 0.9 to 1. This makes selecting the threshold more challenging.

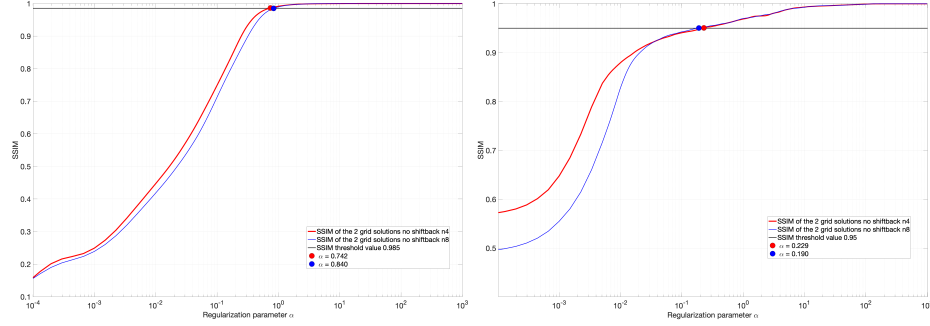


Figure 11: Dual-grid method for parameter choice for the case of the books images shown in 3. Plotted is the SSIM function between the two solutions $\text{SSIM}(\mathbf{g}^{(\alpha)}, \mathbf{f}^{(\alpha)})$ for two regularizers and two noise amplitudes. Left: Tikhonov regularization. The first regularization parameter after the selected threshold value is $\alpha = 0.742$ for the case with less noise (red curve) and $\alpha = 0.84$ for the higher noise case (blue curve). Right: total variation regularization. The first regularization parameter after the selected threshold value is $\alpha = 0.229$ for the case with less noise (red curve) and $\alpha = 0.19$ for the higher noise case (blue curve).

3.2.5 Example reconstructions



Figure 12: Books images and reconstructions with regularization parameter values selected with dual-grid method as seen in Figure 11. First row: "Ground truth" sharp image (ISO100), Blur+little noise, Tikhonov, TV. Second row: "Ground truth" sharp image (ISO100), blur+more noise, Tikhonov, TV (Tikh threshold .985, TV threshold .95)



Figure 13: Books images from Figure 12 cropped for more detailed look. First row: "Ground truth" sharp image (ISO100), blur+little noise, Tikhonov, TV. Second row: "Ground truth" sharp image (ISO100), blur+more noise, Tikhonov, TV (Tikh threshold .985, TV threshold .95)

3.3 Comparison with discrepancy principle parameter choice

To have a comparison to another parameter choice method we use the discrepancy principle. The goal is to find the parameter value α so that the regularized solution $\mathbf{f}^{(\alpha)}$ has a residual norm comparable to the noise level δ in the data \mathbf{m} . For this we define

$$\Psi(\alpha) := \|\mathbf{p} \star \mathbf{f}^{(\alpha)} - \mathbf{m}\|_F \quad (15)$$

and take the discrepancy-based parameter to be the α for which $\Psi(\alpha) \approx \delta$.

For the noise estimation we first sampled 4 constant valued areas of each of the test images and computed the standard deviation σ of the pixel values in these regions. Then we calculated the mean of these values. To get the final noise estimate δ we multiply the mean std value with the square root of the number of pixels in that image, $\delta = \sigma_{mean} \sqrt{n \times n}$. We can then plot the residual norm for each α and see when it matches the noise estimate.

The discrepancy plots for the simulated image example in Figure 14 show clear intersections with the estimated noise for both noise levels in both the Tikhonov regularization case and the total variation regularization case. The according reconstructions compared to the dual-grid method can be seen in Figure 15 for the lower noise case and in Figure 16 for the higher noise case. In both Tikhonov regularization cases the discrepancy principle gives us a lower parameter value than the proposed dual-grid method and for Total variation regularization the discrepancy principle gives us higher parameter values in comparison to the dual-grid method. All the parameter values are also visible in Table 1.

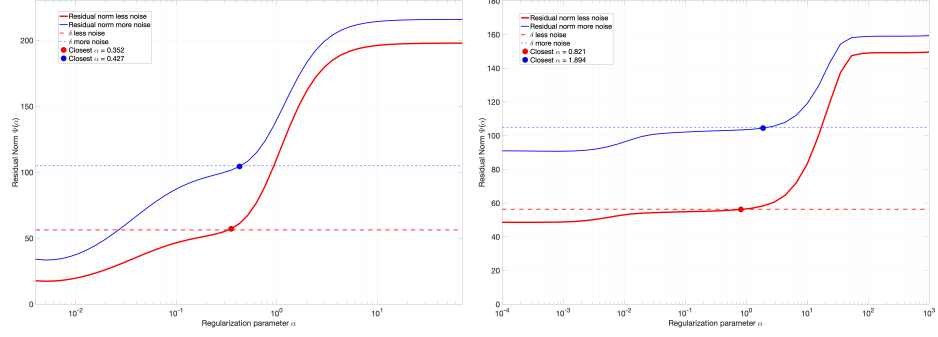


Figure 14: Discrepancy principle for parameter choice for the case of simulated images shown in Figure 1. Plotted is the function $\Psi(\alpha)$ defined in (15) for two regularizers and two noise amplitudes. Left: Tikhonov regularization. The closest regularization parameter to the estimated noise level δ is $\alpha = 0.352$ for the case with less noise (red curve) and $\alpha = 0.427$ for the higher noise case (blue curve). Right: total variation regularization. The closest regularization parameter to the estimated noise level δ is $\alpha = 0.821$ for the case with less noise (red curve) and $\alpha = 1.894$ for the higher noise case (blue curve).

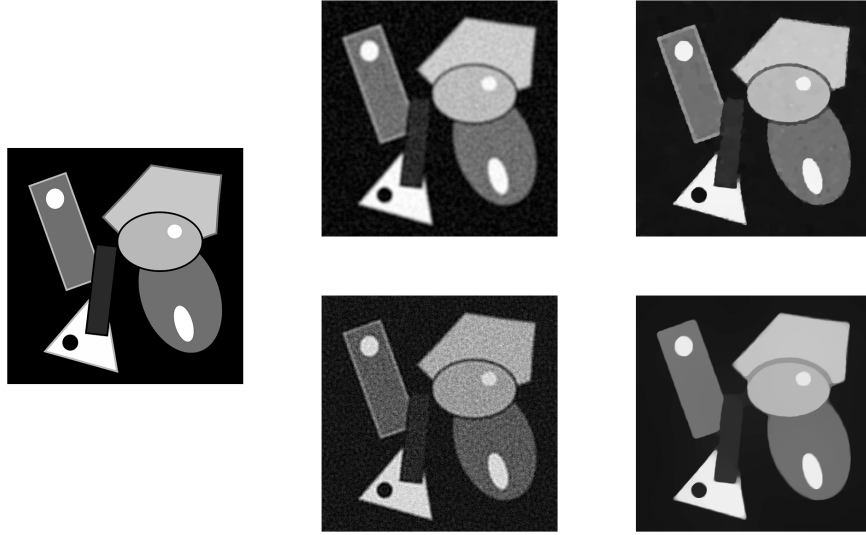


Figure 15: Comparison of optimal reconstructions according to dual-grid method and discrepancy principle for the simulated image with noise level 4%. Left: Ground truth. Upper row dual-grid. Lower row discrepancy principle.

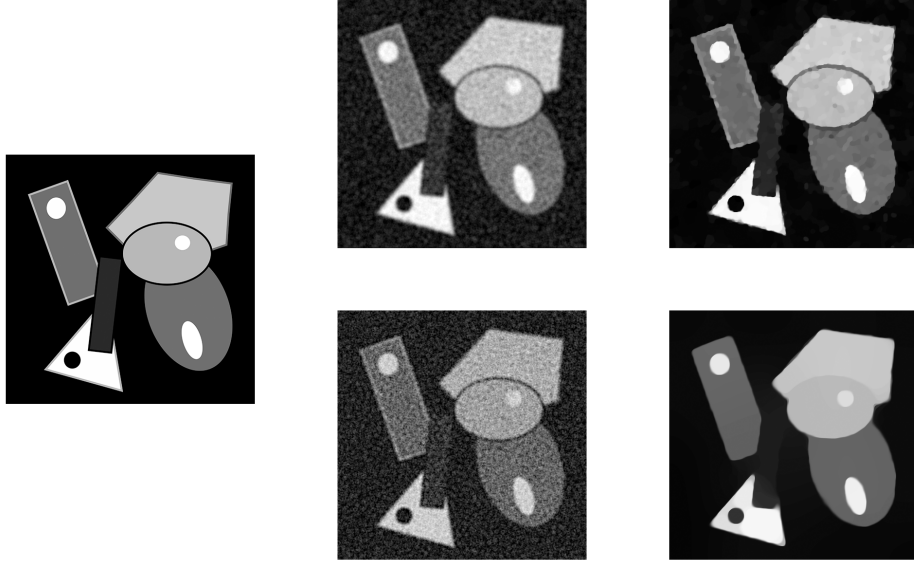


Figure 16: Comparison of optimal reconstructions according to dual-grid method and discrepancy principle for the simulated image with noise level 8%. Left: Ground truth. Upper row dual-grid. Lower row discrepancy principle.

The discrepancy plots for the playing card image example intersect with the estimated noise level only for the Tikhonov regularized case for the higher noise level in Figure 17. The lower noise Tikhonov curve and both total variation regularization cases in figure fail to give us a parameter choice. The parameter value is significantly smaller than we get with the dual-grid method. All the parameter values can be compared in Table 1.

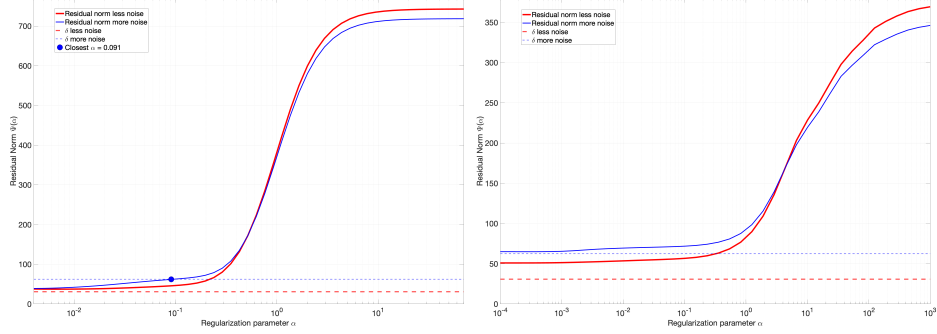


Figure 17: Discrepancy principle for parameter choice for the case of the playing card images shown in Figure 2. Plotted is the function $\Psi(\alpha)$ defined in (15) for two regularizers and two noise amplitudes. Left: Tikhonov regularization. We only get a parameter value for the higher noise case. The closest value to the intersection with the estimated noise level is $\alpha = 0.091$ for the higher noise case (blue curve). Right: total variation regularization. The discrepancy principle fails to give us parameter values for the estimated noise levels.

The discrepancy plots for the books image example in figure 18 show intersections with the estimated noise for both noise levels in the Tikhonov regularization case seen. In the total variation regularization case we get a α value but only in the larger noise case. All the parameter values can be seen in Table 1.

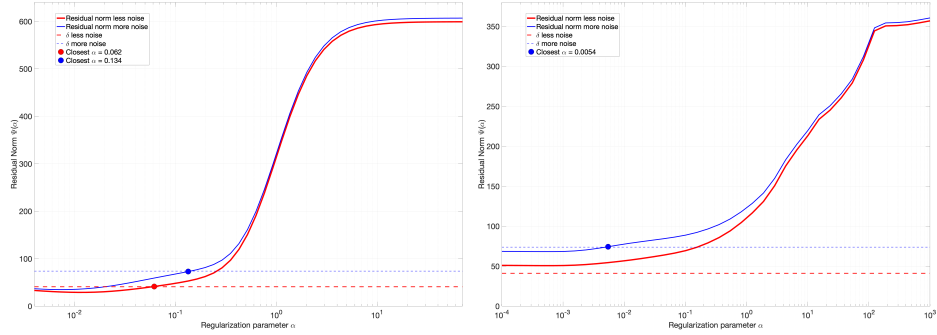


Figure 18: Discrepancy principle for parameter choice for the case of the books images shown in Figure 3. Plotted is the function $\Psi(\alpha)$ defined in (15) for two regularizers and two noise amplitudes. Left: Tikhonov regularization. The closest regularization parameter to the estimated noise level δ is $\alpha = 0.062$ for the case with less noise (red curve) and $\alpha = 0.134$ for the higher noise case (blue curve). Right: total variation regularization. We fail to find a parameter value for the case with less noise (red curve). The closest regularization parameter to the estimated noise level δ is $\alpha = 0.0054$ for the higher noise case (blue curve).

Image test	Tikh. discrep. α	Tikh. Dual α	TV discrep. α	TV Dual α
Simulated 4%	0.352	1.076	0.821	0.085
Simulated 8%	0.427	1.467	1.894	0.158
Queen low	-	0.742	-	0.168
Queen high	0.091	0.616	-	0.085
Books low	0.062	0.742	-	0.229
Books high	0.134	0.840	0.005	0.190

Table 1: Optimal parameter values α for all image examples for the discrepancy principle and the proposed dual-grid method.

4 Discussion

The parameter selection approach we propose is quite flexible in principle. The shifted grid idea can be used with any forward model, not only convolution. The regularization term can also take many forms, including others than the Tikhonov and TV types considered here. The data fidelity norm and image similarity measures can be changed as well within the same parameter choice framework. Detailed assumptions on all of these choices while guaranteeing unique and useful parameter choices are outside the scope of this paper.

A particular strength of our method is that the noise amplitude is not needed. This is a great advantage in real data cases. As we saw in the comparison section 3.3, estimating the noise amplitude may lead to difficulties with traditional parameter choice methods such as the discrepancy principle.

Our experimental results show that the dual-grid method works for the image deblur problem with both simulated and real data. We do need to select the threshold value in our approach. This selection is influenced at least by the regularizer and the amount of fine textures in the image. With a fixed application and specific end-users’ needs, a suitable threshold can be found by experimentation and then kept in subsequent work.

The slight blurring effect of the shift operator does not cause problems as it is only used to determine an optimal parameter. In other words, one would not use the shifted reconstruction as the final solution as it has additional blur.

We noticed a curious effect in our computational experiments. For the real image data, the dual-grid method may give a larger regularization parameter for lower noise than for higher noise. This happened in both TV regularization experiments and for the playing card image with Tikhonov regularization. This seems counter-intuitive as we would expect more regularization with larger noise levels. However, all the resulting reconstructions appear to be reasonable good.

In the detailed books images 13 we see how the TV parameter is too large: we lose some of the small details. This shows that it can be tricky to choose the threshold based on the dual-grid SSIM-curve if the shape is not a nice sigmoid.

References

- [1] Stephan W Anzengruber and Ronny Ramlau. Morozov’s discrepancy principle for tikhonov-type functionals with nonlinear operators. *Inverse Problems*, 26(2):025001, 2009.
- [2] Antonin Chambolle and Thomas Pock. A first-order primal-dual algorithm for convex problems with applications to imaging. *Journal of mathematical imaging and vision*, 40:120–145, 2011.
- [3] Ke Chen, E Loli Piccolomini, and Fabiana Zama. An automatic regularization parameter selection algorithm in the total variation model for image deblurring. *Numerical Algorithms*, 67:73–92, 2014.
- [4] Christian Clason, Bangti Jin, and Karl Kunisch. A duality-based splitting method for ℓ^1 -tv image restoration with automatic regularization parameter choice. *SIAM Journal on Scientific Computing*, 32(3):1484–1505, 2010.
- [5] Elisa Davoli, Rita Ferreira, Irene Fonseca, and José A Iglesias. Dyadic partition-based training schemes for tv/tgv denoising. *Journal of Mathematical Imaging and Vision*, pages 1–39, 2024.
- [6] Yiqiu Dong, Michael Hintermüller, and M Monserrat Rincon-Camacho. Automated regularization parameter selection in multi-scale total variation models for image restoration. *Journal of Mathematical Imaging and Vision*, 40:82–104, 2011.
- [7] Heinz Werner Engl, Martin Hanke, and Andreas Neubauer. *Regularization of inverse problems*, volume 375. Springer Science & Business Media, 1996.
- [8] Keijo Hamalainen, Aki Kallonen, Ville Kolehmainen, Matti Lassas, Kati Niinimäki, and Samuli Siltanen. Sparse tomography. *SIAM Journal on Scientific Computing*, 35(3):B644–B665, 2013.
- [9] Per Christian Hansen. Analysis of discrete ill-posed problems by means of the l-curve. *SIAM review*, 34(4):561–580, 1992.
- [10] Per Christian Hansen, James G Nagy, and Dianne P O’leary. *Deblurring images: matrices, spectra, and filtering*. SIAM, 2006.
- [11] Stefan Kindermann, Lawrence D Mutimbu, and Elena Resmerita. A numerical study of heuristic parameter choice rules for total variation regularization. *Journal of Inverse and Ill-Posed Problems*, 22(1):63–94, 2014.
- [12] Mark A Lukas. Strong robust generalized cross-validation for choosing the regularization parameter. *Inverse Problems*, 24(3):034006, 2008.
- [13] Alexander Meaney, Mikael AK Brix, Miika T Nieminen, and Samuli Siltanen. Image reconstruction in cone beam computed tomography using controlled gradient sparsity. *arXiv preprint arXiv:2412.07465*, 2024.

- [14] Kati Niinimäki, Matti Lassas, Keijo Hamalainen, Aki Kallonen, Ville Kolehmainen, Esa Niemi, and Samuli Siltanen. Multiresolution parameter choice method for total variation regularized tomography. *SIAM journal on imaging sciences*, 9(3):938–974, 2016.
- [15] Stanley Osher, Martin Burger, Donald Goldfarb, Jinjun Xu, and Wotao Yin. An iterative regularization method for total variation-based image restoration. *Multiscale Modeling & Simulation*, 4(2):460–489, 2005.
- [16] Monica Pragliola, Luca Calatroni, Alessandro Lanza, and Fiorella Sgallari. Admm-based residual whiteness principle for automatic parameter selection in single image super-resolution problems. *Journal of Mathematical Imaging and Vision*, 65(1):99–123, 2023.
- [17] Zenith Purisha, Sakari S Karhula, Juuso H Ketola, Juho Rimpeläinen, Miika T Nieminen, Simo Saarakkala, Heikki Kröger, and Samuli Siltanen. An automatic regularization method: An application for 3-d x-ray micro-ct reconstruction using sparse data. *IEEE transactions on medical imaging*, 38(2):417–425, 2018.
- [18] Zenith Purisha, Juho Rimpeläinen, Tatiana Bubba, and Samuli Siltanen. Controlled wavelet domain sparsity for x-ray tomography. *Measurement Science and Technology*, 29(1):014002, 2017.
- [19] L.I. Rudin and S. Osher. Total variation based image restoration with free local constraints. In *Proceedings of 1st International Conference on Image Processing*, volume 1, pages 31–35 vol.1, 1994.
- [20] A.N. Tikhonov. On the solution of ill-posed problems and the method of regularization. *Dokl. Akad. Nauk SSSR*, 1963.
- [21] Alina Toma, Bruno Sixou, and Françoise Peyrin. Iterative choice of the optimal regularization parameter in tv image restoration. *Inverse Probl. Imaging*, 9(4):1171–1191, 2015.
- [22] C.R. Vogel and M.E. Oman. Fast, robust total variation-based reconstruction of noisy, blurred images. *IEEE Transactions on Image Processing*, 7(6):813–824, 1998.
- [23] Yilun Wang, Junfeng Yang, Wotao Yin, and Yin Zhang. A new alternating minimization algorithm for total variation image reconstruction. *SIAM Journal on Imaging Sciences*, 1(3):248–272, 2008.
- [24] Zhou Wang, A.C. Bovik, H.R. Sheikh, and E.P. Simoncelli. Image quality assessment: from error visibility to structural similarity. *IEEE Transactions on Image Processing*, 13(4):600–612, 2004.
- [25] You-Wei Wen and Raymond H Chan. Parameter selection for total-variation-based image restoration using discrepancy principle. *IEEE Transactions on Image Processing*, 21(4):1770–1781, 2011.

- [26] You-Wei Wen and Raymond Honfu Chan. Using generalized cross validation to select regularization parameter for total variation regularization problems. *Inverse Problems and Imaging*, 12(5):1103–1120, 2018.